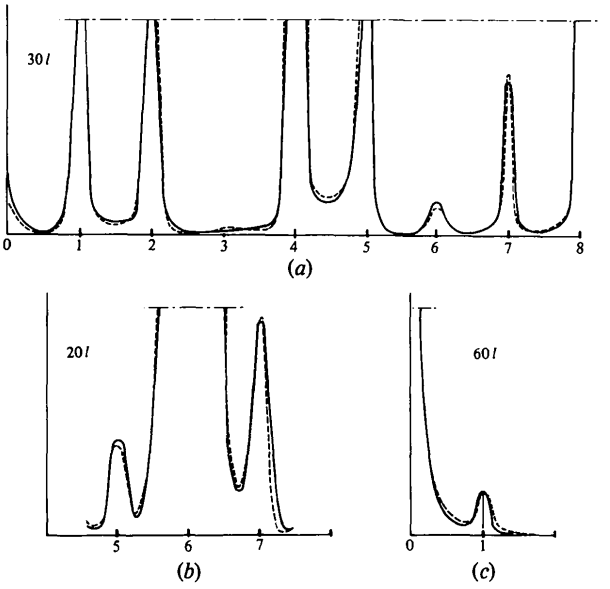

Fig. 7. Diffraction function observed (full lines) and calculated (dashed lines) for (*a*) a superstructure row, (*b*) a broadened substructure row and (*c*) a non-perturbed substructure reflection. Lorentz polarization corrections were made but no absorption correction was taken into account.

notation. In any case this does not modify the α value because it was determined from the streaks between Bragg reflections in regions where (4) only varies very smoothly and is not sensitive to the integration effect. The results are graphically shown in Fig. 7.

6. Conclusion

We have shown that the microtwin observed in 3*c*-type Fe_7S_8 crystals can be simply explained by a planar fault of the same type as the one encountered in hexagonal close packing which exchanges the different threefold axis and modifies, at the fault, the fundamental stacking of the NiAs-type structure.

Let us point out further that this fault is present in all the 3*c*-type Fe_7S_8 crystals we have examined, and moreover with about the same fault rate. It is also present, in addition to $Ni_{17}S_{18}$, in the few crystals of monoclinic 4*c*-type Fe_7S_8 we obtained by vapour transport. But the problem is complicated in the latter case by an additional macrotwinning due to the monoclinic deformation ($\gamma = \pm 89{\cdot}63°$). The Bragg peaks from each of these domains are generally separated and in each domain a microtwinning with diffuse streaks almost identical to the ones of 3*c*-type Fe_7S_8 is observed.

It is noted that in the Fe–S phase diagram the kind of planar fault described above is specific for compositions close to Fe_7S_8 and that it disappears when the iron content increases and then gives rise to other faults which do not perturb the average lattice.

References

BERTAUT, E. F. (1953). *Acta Cryst.* **6**, 557–561.

COLLIN, G., CHAVANT, C. & COMÈS, R., (1983). *Acta Cryst.* B**39**, 289–296.

COWLEY, J. M. (1976*a*). *Acta Cryst.* A**32**, 83–87.

COWLEY, J. M. (1976*b*). *Acta Cryst.* A**32**, 88–91.

COWLEY, J. M. & AU, A. Y. (1978). *Acta Cryst.* A**34**, 738–743.

FLEET, M. E. (1971). *Acta Cryst.* B**27**, 1864–1867.

MUKHERJEE, B. (1969). *Acta Cryst.* B**25**, 673–676.

NAKANO, A., TOKONAMI, M. & MORIMOTO, N. (1979). *Acta Cryst.* B**35**, 722–724.

NAKAZAWA, H., MORIMOTO, M. & WATANABE, E. (1975). *Am. Mineral.* **60**, 359–366.

OVANESYAN, N. S., TRUKHTANOV, V. A., ODINETS, G. Y. & NOVOKOV, G. V. (1971). *Sov. Phys. JETP*, **33**, 1193–1197.

TOKONAMI, M., NISHIGUSHI, K. & MORIMOTO, N. (1972). *Am. Mineral.* **57**, 1066–1068.

VAN LANDUYT, J. & AMELINCKX, S. (1972). *Mater. Res. Bull.* **7**, 71–80.

Acta Cryst. (1983). B**39**, 303–306

Bonding in Lithium Tetrafluoroberyllate(II)

BY D. M. COLLINS, M. C. MAHAR AND F. W. WHITEHURST

Department of Chemistry, Texas A&M University, College Station, Texas 77843, *USA*

(*Received* 8 *June* 1982; *accepted* 10 *December* 1982)

Abstract

The electron deformation density of Li_2BeF_4 has been investigated with regard to the bonding description of McGinnety [*J. Chem. Phys.* (1972), **59**, 3442–3443]. Data in the range $0 < \sin\theta/\lambda \leq 1{\cdot}20$ Å^{-1} were obtained in a single-crystal X-ray diffraction experiment ($R = 0{\cdot}021$ for 984 unique reflections) and used to represent the deformation density in *X*–*X* maps. The results conform to the expected covalent character associated with Be–F bonds but offer no support for the proposed Li–F covalent bonding.

0108-7681/83/030303-04$01.50

Introduction

McGinnety (1972) has rationalized the distortion of the tetrahedral arrangement of F atoms about Be in the Li_2BeF_4 crystal structure in terms of crystal force fields. Assuming a change in bond length to be proportional to the force acting upon that bond, McGinnety used the observed bond lengths established by Burns & Gordon (1966) and several sets of charges associated with the various atoms of the structure to derive force constants for the bonds. The calculated force constants were compared to those determined by means of vibrational spectroscopy, thus giving an estimate of the correct set of charges to be assigned to the atoms. The study showed that the charge associated with the F atoms corresponded to Be–F covalent bonding as well as ionic bonding. These calculations also suggested the existence of covalent character in Li–F bonds. Experimental support for McGinnety's results can be sought through the examination of charge density in electron deformation density maps. For bonds between first-row atoms the deformation density maps should show accumulation of charge density between atomic centers in cases where covalent bonding or mutual sharing of electrons is taking place. In the situation where the bonding is ionic we should expect little, if any, deformation density on the bond axis. In this paper, we present the pertinent results from our study of the deformation density of Li_2BeF_4.

McGinnety (1972) used as a structure model for his calculations the coordinates established by the X-ray diffraction study of Burns & Gordon (1966). Because the data of Burns & Gordon did not go beyond $\sin\theta/\lambda \simeq 0.70$ Å^{-1}, we have redetermined the structure of Li_2BeF_4 using data collected to an upper limit of $\sin\theta/\lambda < 1.20$ Å^{-1}. The first section of this report will describe our data collection and refinement. In the second section we will discuss the results.

Structure redetermination

Crystals of Li_2BeF_4 were supplied for us by Dr John Burns of Oak Ridge National Laboratories. The crystal chosen for data collection was ground to an approximately spherical shape with its diameter varying between 0·25 and 0·30 mm; absorption effects, which were ignored, could give rise to not more than 0·3% relative error in any structure factor. Monochromatized Mo $K\alpha$ radiation was used for measuring intensities by the $\theta/2\theta$-scan method on a Syntex $P\bar{1}$ diffractometer. Measurements in the 2θ range 0·1 to 69·3° were made for two symmetry-equivalent regions, the agreement between the two being measured by $R = 0.023$. For the 2θ range 69·3 to 117·04°, data were collected in one region. From the entire 2θ range 984 unique reflections were retained as significant measurements by a 3σ counting-statistics criterion. The experimental conditions are summarized in Table 1.

The atomic coordinates, anisotropic thermal parameters, a coefficient for correction of secondary-extinction effects (Becker & Coppens, 1974) and an overall scale factor were refined using all unique reflections. The function minimized was $\sum w(|F_o| - |F_c|)^2$ with experimental weights based upon counting statistics and atomic scattering factors taken from *International Tables for X-ray Crystallography* (1974). The final value for $R = \sum||F_o| - |F_c||/\sum|F_o|$ was 0·021 for this refinement. In a subsequent high-angle refinement the scale factor and extinction corrections were held constant and the 535 unique data in the $\sin\theta/\lambda$ range 0·60 to 1·20Å^{-1} were used to refine the 63 thermal-motion and position coordinates to their final values given in Table 2. The final structure model based

Table 1. *Experimental data for the X-ray diffraction study of crystalline* Li_2BeF_4

(*a*) Crystal parameters at 300 K
Space group: $R\bar{3}$
Hexagonal cell: $a = 13.310$ (6), $c = 8.908$ (3) Å
$F(000) = 828$

(*b*) Measurement of intensity data
Diffractometer: Syntex $P\bar{1}$
Radiation: Mo $K\alpha$ ($\lambda = 0.71073$ Å)
Monochromator: highly oriented graphite crystal

	(I)	(II)
2θ range	0·1 to 69·3°	69·3 to 117·04°
Scan type	$\theta/2\theta$	$\theta/2\theta$
Scan speed (in 2θ)	2·0 to 16·0° min^{-1}	0·8 to 16·0° min^{-1}

Background measurement: at the beginning and end of 2θ scan, each for half the time taken for 2θ scan
Standard reflections: 3 after every 97 reflections: no significant changes in intensity were observed
Extinction model: isotropic, type 1 (Lorentzian); $g = 0.122\ (12) \times 10^{-4}$; maximum correction = 15% on $|F|$

Table 2. *Fractional coordinates in the unit cell and thermal parameters* (Å^2) *for* Li_2BeF_4

Numbers in parentheses denote standard deviation in the last significant figure.

	F(1)	F(2)	F(3)	F(4)	Be	Li(1)	Li(2)
x	0·10566 (7)	0·32319 (7)	0·20351 (8)	0·20914 (9)	0·21158 (13)	0·21486 (25)	0·20727 (25)
y	−0·11053 (7)	0·00601 (7)	0·07500 (8)	0·08194 (8)	0·01538 (11)	0·02098 (23)	0·01648 (22)
z	0·25200 (10)	0·24871 (10)	0·10422 (8)	0·39230 (8)	0·24931 (14)	0·58112 (25)	−0·08507 (27)
U_{11}	0·0148 (3)	0·0126 (2)	0·0248 (3)	0·0254 (3)	0·0142 (4)	0·0189 (9)	0·0203 (9)
U_{22}	0·0137 (3)	0·0155 (3)	0·0165 (3)	0·0184 (3)	0·0132 (5)	0·0188 (9)	0·0178 (9)
U_{33}	0·0154 (2)	0·0201 (3)	0·0102 (2)	0·0107 (2)	0·0103 (4)	0·0141 (7)	0·0143 (7)
U_{12}	0·0021 (2)	0·0076 (2)	0·0125 (2)	0·0142 (3)	0·0072 (4)	0·0101 (7)	0·0103 (7)
U_{13}	−0·0003 (2)	−0·0002 (2)	−0·0003 (2)	−0·0011 (2)	−0·0002 (3)	0·0009 (7)	0·0003 (7)
U_{23}	0·0012 (2)	−0·0009 (2)	0·0015 (2)	−0·0021 (2)	−0·0002 (3)	−0·0002 (6)	0·0004 (6)

Table 3. *Selected bond parameters (distances in* Å*) in* Li_2BeF_4

This adaptation of Table 4 of Burns & Gordon (1966) is based on the position coordinates given in Table 2. Estimated standard deviations ($\times 10^3$) are given in parentheses.

Be–F(1)	1·558 (2)	Li(1)–F(1′)	1·860 (2)	Li(2)–F(1′)	1·868 (3)
F(2)	1·549 (2)	F(2′)	1·865 (3)	F(2′)	1·851 (3)
F(3)	1·548 (2)	F(4)	1·885 (2)	F(3′)	1·856 (3)
F(4)	1·561 (2)	F(4′)	1·891 (3)	F(3)	1·868 (3)

on this high-angle refinement gave $R = 0{\cdot}023$ for the 535 reflections used in the refinement, and $R = 0{\cdot}022$ for all reflections.* There is no chemically significant difference between our new values and those reported by Burns & Gordon (1966) although the current description replaces the former x,y by $\bar{y},\bar{x}$ respectively. Selected interatomic distances are given in Table 3.

Results

As described earlier (Burns & Gordon, 1966), the F atoms are located about Be and Li in tetrahedral arrangements. The fact that the tetrahedra were irregular led McGinnety (1972) to investigate the forces acting on the Be–F and Li–F tetrahedra, which in turn led to a description of the charge density associated with the atoms in these tetrahedra. His determination of less than the expected charge on the anion F^- suggests more sharing of electrons on the part of the fluorine or a partial covalent character in the bonds in which fluorine takes part.

Deformation density maps should show an accumulation of charge in the bonding region between atoms engaged in covalent bonding (Coppens & Stevens, 1977). Figs. 1 and 2 present the appropriate deformation density maps as sections at $z = 0{\cdot}75$ and $x = 0{\cdot}22$. The maps are of the standard type in which the promolecule is assumed to be made up of suitably placed neutral, isolated Hartree–Fock atoms that are rigid and characterized by the thermal-motion coordinates of the structure model. The data employed in the synthesis are drawn from the sin θ/λ region 0·0 to 0·8 Å^{-1} (Stewart, 1976), each measurement taken as the average of symmetry-equivalent observations. An estimated standard deviation of deformation density in the region dominated by observational error, the region of points greater than 0·5 Å from any nucleus (Lehmann, 1980), was calculated as the root mean square of the deformation density with rejection of outliers at the 95% confidence level. The value, $\sigma = 0{\cdot}07$ e Å^{-3}, is comparable to, but larger than an *a priori* estimate of 0·03 e Å^{-3} following Stevens & Coppens (1976) and Coppens & Stevens (1977).

* A list of structure factors has been deposited with the British Library Lending Division as Supplementary Publication No. SUP 38273 (9 pp.). Copies may be obtained through The Executive Secretary, International Union of Crystallography, 5 Abbey Square, Chester CH1 2HU, England.

The maps show the anticipated charge accumulation between Be and F centers and consequently lend support to McGinnety's Be–F bonding description. Fig. 1 represents charge density in contours at intervals of $\sigma(0{\cdot}074$ e Å$^{-3})$ on the plane $x = 0{\cdot}22$ which passes approximately through the bonding regions of Be–F(3), Be–F(4), Li(1)–F(4), Li(1)–F(1′), Li(2)–F(1′), and Li(2)–F(3). The charge accumulation associated with the Be–F axes shows peaks with charge density maxima of ~0·42 e Å^{-3} about midway between bonded Be and F, but in both cases apparently polarized toward Li. There is, nevertheless, little, if any, charge density between the Li and F centers. The charge density region to the left of F(1) represents charge density along a Be–F bond for which the Be lies just above the plane of the figure; the projected Be position has been noted on the map.

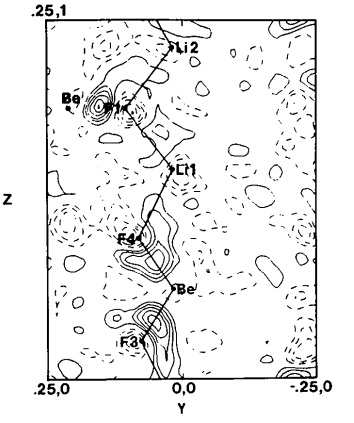

Fig. 1. Level $x = 0{\cdot}22$ showing Be–F(4), Be–F(3), Li(1)–F(1′), Li(1)–F(4), Li(2)–F(3), and Li(2)–F(1′) interatomic-region charge density. Contour levels are at intervals of $\sigma(0{\cdot}074$ e Å$^{-3})$ with the 0·0 e Å^{-3} contour not shown, positive contours as solid lines, negative contours as dashed lines.

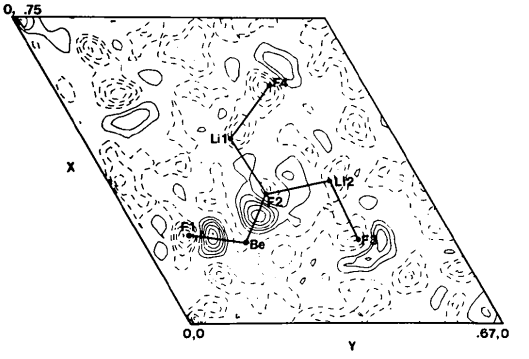

Fig. 2. Level $z = 0{\cdot}75$ showing Be′–F(1′), Be′–F(2′), Li(1′)–F(2′), Li(1′)–F(4′), Li(2′)–F(3′), and Li(2′)–F(2′) interatomic-region charge density. Contour levels are at intervals of $\sigma(0{\cdot}074$ e Å$^{-3})$ with the 0·0 e Å^{-3} contour not shown, positive contours as solid lines, negative contours as dashed lines.

Fig. 2 represents charge density in contours at intervals of $\sigma(0{\cdot}074$ e Å$^{-3})$ on the plane $z = 0{\cdot}75$. The interatomic axes Be′–F(1′), Be′–F(2′), Li(1′)–F(4′), Li(1′)–F(2′), Li(2′)–F(2′), and Li(2′)–F(3′) lie approximately on this plane. The deformation density features associated with the Be–F(1) and Be–F(2) bonds have maxima of about 0·42 e Å^{-3} and features similar to those seen in Fig. 1. As in Fig. 1, there appears to be little or no localization of charge deformation density on the Li–F bond axes.

McGinnety (1972) has suggested the Li–F bonding interactions may have covalent character. In the figures which display the deformation density along the (approximate) axis of each type of interaction, only Li(1)–F(4) has substantial density symmetrically disposed about its axis. Because the density pattern has its maximum less than 0·5 Å from F, and in any case does not rise as high as 3σ, this feature cannot be considered significant. By the pattern of no significant charge accumulation or localization in the Li–F bonds, the diffraction data fail to support the suggestion that covalent character associated with the Li–F bond is significant.

Conclusion

Charge deformation density provides direct experimental support of McGinnety's (1972) prediction of covalent character for the Be–F bonds. The corresponding deformation density features are significant point-by-point at better than 3σ and the overall patterns are unambiguously recognizable as typical of covalent bonding between the lighter elements with orbitals of *s* and *p* character. On the other hand, we have not been able to evince clear indications of the suggested covalency in Li–F bonds.

We wish to thank Dr John H. Burns of the Oak Ridge National Laboratories for his encouragement and the Li_2BeF_4 crystals necessary for this work and Dr Larry Falvello for his assistance in the structure redetermination. This work was supported in part by Grant A-742 from the Robert A. Welch Foundation.

References

BECKER, P. J. & COPPENS, P. (1974). *Acta Cryst.* A**30**, 129–147.
BURNS, J. H. & GORDON, E. K. (1966). *Acta Cryst.* **20**, 135–138.
COPPENS, P. & STEVENS, E. (1977). *Adv. Quantum Chem.* **10**, 1–35.
International Tables for X-ray Crystallography (1974). Vol. IV, edited by J. A. IBERS & W. C. HAMILTON. Birmingham: Kynoch Press.
LEHMANN, M. S. (1980). In *Electron and Magnetization Densities in Molecules and Crystals*, edited by P. BECKER. New York: Plenum.
MCGINNETY, J. A. (1972). *J. Chem. Phys.* **59**, 3442–3443.
STEVENS, E. D. & COPPENS, P. (1976). *Acta Cryst.* A**32**, 915–917.
STEWART, R. F. (1976). *Acta Cryst.* A**32**, 565–574.

Acta Cryst. (1983). B**39**, 306–311

Lattice Modulation in the Long-Period Superstructure of Cu_3Sn

BY Y. WATANABE, Y. FUJINAGA AND H. IWASAKI*

The Research Institute for Iron, Steel and Other Metals, Tohoku University, Sendai 980, *Japan*

(*Received* 1 *November* 1982; *accepted* 15 *December* 1982)

Abstract

An X-ray diffraction investigation has been made on single crystals of Cu_3Sn having a periodic antiphase domain structure based on the Cu_3Ti-type ordered lattice. Refinement of the structure has shown that most of atoms are not located exactly on the sites of the basic lattice but are displaced with a largest magnitude of 0·126 Å. The displacements of the atoms consist of two parts having different characteristics. One has its component in the direction of the long period and is opposite in sense for Cu and Sn atoms. This characteristic is the same as that of the displacements of atoms found in the periodic antiphase domain structures based on the $L1_2$- and $L1_0$-type ordered lattices and this identity suggests that electron charge density waves are responsible for its production. The other part has its components in both the long-period direction and the direction perpendicular to it and is observed only for Cu atoms; the origin for this can be found in the marked disparity in sizes between the two sorts of atoms. [Crystal data: $Cu_{75{\cdot}5}Sn_{24{\cdot}5}$, orthorhombic, *Cmcm*, $a = 5{\cdot}529$ (8), $b = 47{\cdot}75$ (6), $c = 4{\cdot}323$ (5) Å, $V = 1141$ (5) Å^3, 80 atoms/cell, $D_x = 8{\cdot}97$ (4) g cm^{-3}, μ(Mo $K\alpha$) = 390·4 cm^{-1}.]

* To whom correspondence should be addressed.

0108-7681/83/030306-06$01.50